

PACS numbers: 51.50+v; 52.38. – r; 42.87.Bg
DOI: 10.1070/QE2007v037n10ABEH013646

Femtosecond laser optical gas breakdown microplasma: the ionisation and postionisation dynamics

V.V. Bukin, S.V. Garnov, A.A. Malyutin, V.V. Strelkov

***Abstract*. The formation and evolution dynamics of the laser plasma produced in the microvolumes of gases (air, nitrogen, argon, and helium) upon their multiple ionisation by high-intensity (4×10^{16} W cm^{-2}) tightly focused (to a region 1.7 μm in diameter) 400-nm, 100-fs second-harmonic pulses from a Ti : sapphire laser is studied. The spatiotemporal distribution profiles of the refractive index and electron microplasma density were recorded by ultrahigh-speed interferometry. The postionisation of a femtosecond laser plasma, i.e. the growth of the electron density known after the end of the exciting laser pulse, is detected for the first time. A theoretical model is proposed, which describes the mechanism of plasma postionisation by hot photoelectrons. The results of electron density calculations are in good agreement with experimental data.**

Keywords: *femtosecond laser microplasma, interferometry*.

1. Introduction

Investigation of a laser microplasma produced in gases and condensed media ionised by ultrashort high-intensity pulses is an important direction in the physics of laser radiation – matter interactions. This problem is topical both from the standpoint of basic science – gaining new experimental data on the properties of extremely nonequilibrium, spatially nonuniform high-density plasma and its formation mechanisms – and in connection with numerous applied problems – development of techniques for the generation of extremely short (attosecond) light pulses, design of short-wavelength radiation sources for nanolithography, improvement of the existing technologies and elaboration of new methods for the high-precision laser micro- and nanostructuring the surface and volume of metals and transparent optical materials.

In this work, we present the results of experimental investigations of the formation and evolution dynamics of the laser microplasma generated in gases by 400-nm, 100-fs, 200-μJ second-harmonic pulses from a Ti : sapphire laser. The plasma was produced in gases (air, nitrogen, argon, and helium) at the atmospheric pressure due to the optical breakdown of the medium by single femtosecond laser pulses focused to a region ~2 μm in diameter. In this case, the 'vacuum' intensity in the beam waist amounted to $\sim 4 \times 10^{16}$ W cm^{-2}. The second harmonic was used because its wavelength falls into the UV spectral range of interest to us and it provides a drastic increase in the excitation contrast ratio, which is very important for the correct performance of experiments in the high-intensity field and the interpretation of the data obtained. The experimental investigations were performed by using the ultrahigh-speed microinterferometry technique, which was developed and employed many times in our works [1 – 7].

V.V. Bukin, S.V. Garnov, A.A. Malyutin, V.V. Strelkov A.M. Prokhorov General Physics Institute, Russian Academy of Sciences, ul. Vavilova 38, 119991 Moscow, Russia; e-mail: garnov@kapella.gpi.ru

Received 26 June 2007
Kvantovaya Elektronika **37** (10) 961 – 966 (2007)
Translated by E.N. Ragozin

2. Ultrahigh-speed interferometry of a femtosecond laser microplasma

The experimental setup is presented schematically in Fig. 1. A single pulse from a Ti : sapphire laser was split in a beamsplitter into two unequal parts – the higher-intensity exciting pulse and the lower-intensity probe pulse. After

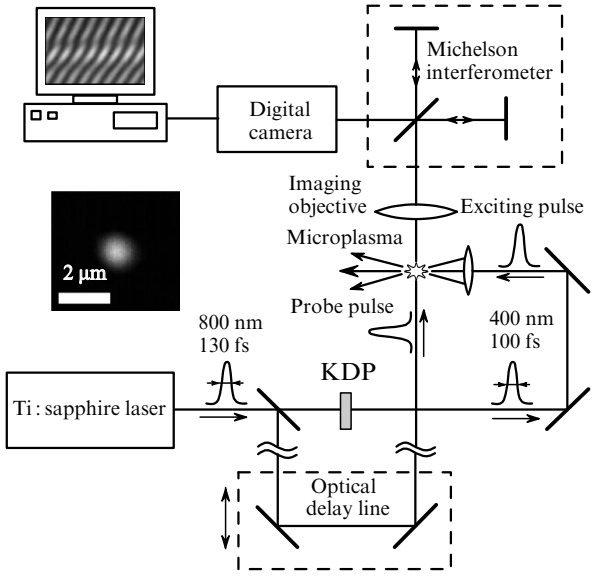

Figure 1. Scheme of the experimental setup for interferometric measurements of the formation and evolution dynamics of a femtosecond laser microplasma. The spatial profile of radiation intensity distribution is measured in the focal plane of the focusing lens.

conversion to the second harmonic in a 1-mm thick KDP crystal, the exciting pulse was focused into the volume of gas under study to produce a microplasma due to optical breakdown in the gas. The nitrogen, argon, and helium plasmas were studied by focusing the laser pulse into a gas jet at the atmospheric pressure. Focusing was performed with a high-quality aspheric lens with the focal length $F = 8$ mm and a numerical aperture NA = 0.5. Figure 1 shows the measured spatial intensity profile of the focused laser radiation. One can see that the field distribution near the focal plane is close to the Gaussian one with a diameter of 1.7 μm (at the $1/e^2$ level).

As mentioned above, the radiation conversion to the second harmonic allowed us to enhance considerably the excitation contrast ratio, which is very important in the investigations of the plasma produced by laser pulses with peak intensities 2–3 orders of magnitude higher than the optical breakdown threshold (which is typically $\sim 10^{14}$ W cm^{-2} for the air, nitrogen, and argon). Because the contrast ratio for the fundamental harmonic radiation measured with a correlator was no less than 100 : 1, after conversion to the second harmonic radiation it increased quadratically to become higher than 1000 : 1. This allowed us to eliminate or minimise the effect of the low-intensity pedestal and of the pre- and postpulses, which are always present in the initial 800-nm radiation of a femtosecond laser.

After reflection from the beamsplitter, the probe pulse passed through a variable optical delay line and propagated through the plasma under study perpendicular to the propagation direction of the exciting pulse. By varying the length of the delay line with the help of a precision stepping motor, we changed the arrival time of the probe pulse into the region under study relative to the exciting pulse. The tuning range was 0–40 ps with a minimal step of 10 fs. The fundamental harmonic of the Ti : sapphire laser was used for probe to provide the highest possible sensitivity of measuring low plasma densities.

At the output of the Michelson interferometer the probe radiation was divided into two coherent beams propagating at a small angle. Because the dimensions of the microplasma were much smaller than the probe-pulse diameter (~ 3 mm), its main part propagated outside the region of induced optical inhomogeneity could be used as a reference beam. In this case, the Michelson interferometer was used to separate the reference and object beams, select the orientation and period of interference fringes, and to compensate for the path difference of the interfering femtosecond pulses.

Recall that all numerous pulsed laser interferometric techniques for plasma diagnostics, which have been used many times earlier and are presently used in numerous experimental works (see for instance, papers [1–3, 7–28] and references therein), are based on the recording of the 'instantaneous' interference patterns of the volume of the excited material (plasma), which are obtained with the help of probe laser 'illumination' pulses delayed in time.

A bending of fringes in the interference patterns corresponds to the phase shift of the probe pulse immediately after its passage through the microplasma (a shift by one fringe corresponds to a phase shift of 2π). The spatial distribution of the phase shift of the probe pulse was reconstructed on the basis of the standard Fourier filtration algorithm [29, 30]. In this case, the sensitivity of phase measurement by this method was $\sim 2\pi/30$, which far exceeds the sensitivity of the 'spatial' method involving the determination of interference fringe coordinates.

The phase of the probe pulse changes due to a change in the refractive index inside the microplasma relative to the refractive index of the unperturbed gas. For a cylindrical symmetry of the plasma object, this change is related to the refractive index distribution by the Abelian transformation. Accordingly, by using the inverse Abelian transformation it is possible to obtain the radial dependence of the refractive index distribution inside the microplasma from the spatial distribution of the phase shift. Because the experimentally recorded profile of the phase shift is always asymmetric, it should be symmetrised. In the processing of a large number of interference patterns, for the symmetrisation procedure in this case we employed an approximation of every cross section by an even function of a certain class using the least squares technique. Within the framework of the Drude

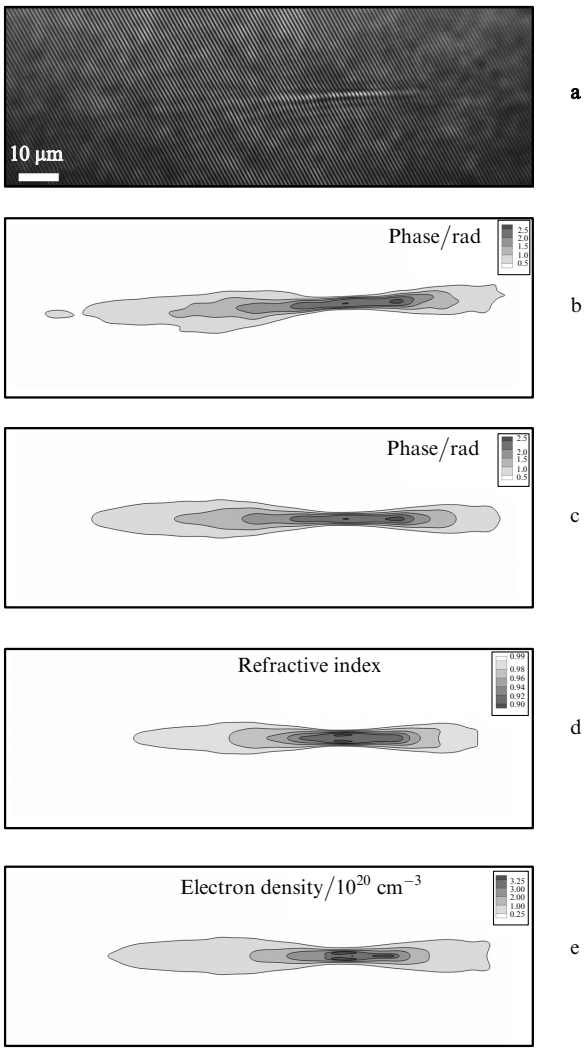

Figure 2. Plasma interferograms and spatial distributions of the density and electron concentraction: interferogram of the air microplasma (the probe pulse delay is 10 ps, the peak intensity of the exciting radiation is 9×10^{15} W cm^{-2}, the exciting radiation propagates from left to right) (a), corresponding phase shift of the probe pulse (b), symmetrised phase shift (c), radial distribution of the refractive index reconstructed on the basis of inverse Abelian transformation (d), and radial distribution of the electron density obtained within the framework of the Drude model (e).

model, the refractive index and the electron density N_e are related by the expression [1, 31, 32]:

$$n = \left[n_0^2 - \left(\frac{\omega_p}{\omega}\right)^2\right]^{1/2} = \left(n_0^2 - \frac{N_e e^2}{\varepsilon_0 m \omega^2}\right)^{1/2}, \quad (1)$$

where $\omega = 2.35 \times 10^{15}$ rad s^{-1} is the angular frequency of the probe radiation; ω_p is the plasma frequency; e and m are the electron charge and mass; and ε_0 is the dielectric constant.

Thus, proceeding from the 'instantaneous' interference patterns of the laser plasma, we obtained the 'instantaneous' spatial distributions of the electron density inside the microplasma. The stages of interference pattern processing listed above are represented in Fig. 2. The interference patterns were processed by using the freely distributed IDEA (Interferometric Data Evaluation Algorithms; http://www.optics.tugraz.at/idea/idea.html) software.

Figure 3a presents the electron density measurement data for nitrogen and argon microplasmas near the focus in the 0 – 5000 fs time range. One can see that the characteristic time of fast plasma formation is about 500 fs; then, the growth in the electron density slows down but does not terminate completely. It is also evident that the duration of the stage of a rapid growth in the electron density virtually corresponds to the duration of laser action, which is determined in this case by the time during which the laser radiation intensity exceeds the threshold intensity of the gas breakdown. For a Gaussian temporal profile, the peak intensity $I_0 = 4 \times 10^{16}$ W cm^{-2}, and the breakdown threshold $I_{th} = 10^{14}$ W cm^{-2} (nitrogen), the duration of laser action is about 300 fs.

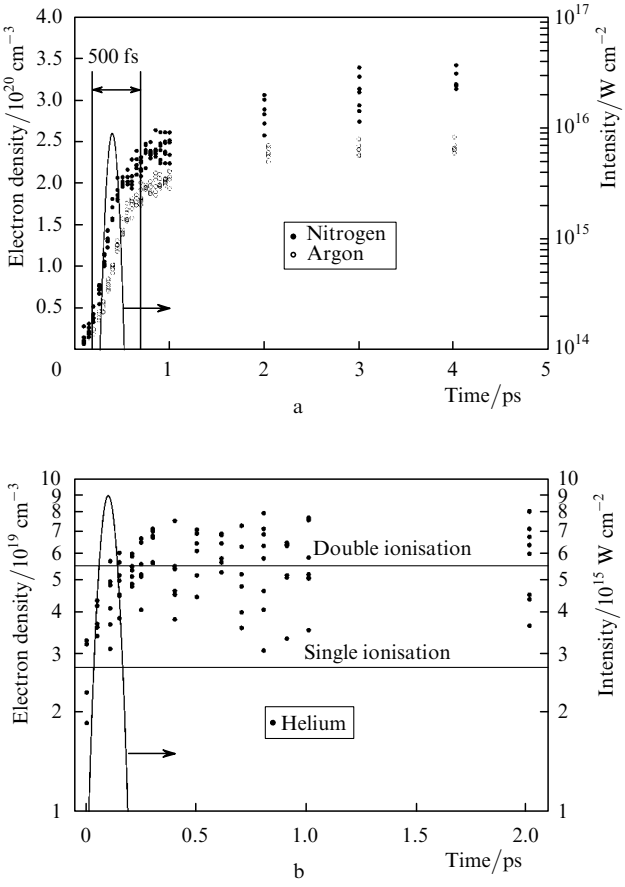

Figure 3. Time dependence of the electron density in the waist (the peak intensity of the exciting pulse is $\sim 9 \times 10^{15}$ W cm^{-2}) measured in nitrogen and argon (a) and in helium (b). The temporal intensity profile of the 100-fs Gaussian beam is shown by the solid curve.

For a helium plasma (Fig. 3b), the duration of rapid plasma formation also corresponds to the period of laser action. The relatively wide scatter in data points is due to the low (at the limit of sensitivity of our technique) electron density of this plasma. One can see from Fig. 3b that upon the optical breakdown of helium under these conditions, the electron plasma density achieves its maximum possible value (doubly ionised helium) in less than 500 fs and then ceases to build up. However, for nitrogen, as follows from Fig. 3a, the electron plasma density continues to increase for a substantially longer time – for several picoseconds, which exceeds the period of plasma interaction with the exciting laser radiation. As far as is known from the literature, earlier this process has never been observed experimentally in the femtosecond laser plasma of an optical breakdown.

3. Theoretical model of femtosecond laser microplasma formation and development

We used the following ionisation mechanism in our experiments: the laser pump pulse ionises the gas and heats the photoelectrons, and then collisional ionisation by hot photoelectrons occurs. Calculations of the electron density dynamics based on this mechanism are consistent with experimental data. The method of our calculations is briefly described below.

3.1 Photoionisation

The photoionisation rate (in atomic units) for an atom or an ion with a charge Z and ionisation energy I_Z is calculated from the expression [32]

$$w_Z(t) = \frac{4E_Z}{E(t)} \exp\left[-\frac{2E_Z}{3E(t)}\right], \quad (2)$$

where

$$E_Z = \left(\frac{I_Z}{\mathrm{Ry}}\right)^{3/2} \quad (3)$$

is the intraatomic (intraion) field intensity and $E(t)$ is the instantaneous intensity of the laser field. In ordinary units, expression (2) is written as

$$w_Z(t) = \frac{4m^3|e|^9 E_Z}{E(t)\hbar^7} \exp\left[-\frac{2m^2|e|^5 E_Z}{3E(t)\hbar^4}\right],$$

where E_Z is defined by expression (3).

Note that a comparison of calculations made by expression (2) with the results of direct numerical integration of the Schrödinger equation in the laser field performed in [33] demonstrates a high accuracy of expression (2).

The densities of atoms $[N_0(t)]$ and ions $[N_Z(t)]$ are calculated by integrating numerically the system of equations:

$$\frac{dN_0}{dt} = -N_0(t)w_0(t),$$

$$\frac{dN_1}{dt} = N_0(t)w_0(t) - N_1(t)w_1(t),$$

$$\ldots \qquad (4)$$

$$\frac{dN_Z}{dt} = N_{Z-1}(t)w_{Z-1}(t) - N_Z(t)w_Z(t),$$

$$\ldots$$

where $N_0(0)$ is the initial atomic density; and $N_Z(0) = 0$ for $Z \geqslant 1$.

This system includes charge states Z, up to those whose photoionisation probability is negligible. We analysed the photoionisation dynamics in air by considering only nitrogen and oxygen and neglecting the contributions made by other gases.

3.2 Laser heating

Recent investigations [34–37] of electron scattering by ions in the presence of the laser field show that electrons may be efficiently heated, in particular, due to multiple correlated collisions of an electron, oscillating in the laser field with the same ion (the 'parachute effect').

We determined the electron temperature by using the approximate analytic expression for the heating rate from [36]. The initial temperature was determined from the average electron energy acquired upon photoionisation. Note that the heating rate derived in [36] saturates with temperature, and therefore the temperature reached during heating depends only slightly on its initial value. Under our conditions, the calculated temperature at the beam focus after heating was about 0.3 keV.

3.3 Ionisation by electron impact

The electron density dynamics following a laser pulse can be calculated by using the known cross sections and rates of collisional ionisation [38–41] and collisional excitation [42–48] for nitrogen atoms and ions.

Note that the temperature dependences of the cross sections for ionisation and excitation are nonresonance in the electron temperature range under study. That is why the inaccuracy in determining the electron temperature with the help of the analytical theory [36] should not lead to fundamental errors in the calculation of the dynamics of collisional ionisation.

A comparison of the cross sections for direct collisional ionisation and collisional excitation shows that under our experimental conditions:

(i) ionisation occurs primarily due to successive excitation rather than direct ionisation;

(ii) the rate of the successive process is primarily determined by the rate of excitation from the ground state, while the further excitation and ionisation proceed faster.

For this reason, the collisional ionisation is simulated by using two (for each Z value) rates: the rate $q_Z^{\mathrm{gr-ex}}$ of excitation from the ground state to an excited state (the state with the highest excitation probability is selected) and the total rate $q_Z^{\mathrm{ex-cont}}$ of all transitions from this state. Therefore, the collisional ionisation dynamics is described by the system of equations:

$$\frac{dN_0^{\mathrm{gr}}}{dt} = -N_0^{\mathrm{gr}} q_0^{\mathrm{gr-ex}}(T),$$

$$\frac{dN_0^{\mathrm{ex}}}{dt} = N_0^{\mathrm{gr}} q_0^{\mathrm{gr-ex}}(T) - N_0^{\mathrm{ex}} q_0^{\mathrm{ex-cont}}(T),$$

$$\frac{dN_1^{\mathrm{gr}}}{dt} = N_0^{\mathrm{ex}} q_0^{\mathrm{ex-cont}}(T) - N_1^{\mathrm{gr}} q_1^{\mathrm{gr-ex}}(T),$$

$$\frac{dN_1^{\mathrm{ex}}}{dt} = N_1^{\mathrm{gr}} q_1^{\mathrm{gr-ex}}(T) - N_1^{\mathrm{ex}} q_1^{\mathrm{ex-cont}}(T),$$

$$\ldots$$

$$\frac{dN_Z^{\mathrm{ex}}}{dt} = N_{Z-1}^{\mathrm{ex}} q_{Z-1}^{\mathrm{ex-cont}}(T) - N_Z^{\mathrm{ex}} q_Z^{\mathrm{gr-ex}}(T), \qquad (5)$$

$$\frac{dN_Z^{\mathrm{ex}}}{dt} = N_Z^{\mathrm{gr}} q_Z^{\mathrm{gr-ex}}(T) - N_Z^{\mathrm{ex}} q_Z^{\mathrm{ex-cont}}(T),$$

$$\ldots$$

$$\frac{dT}{dt} = -\frac{2}{3\tilde{N}_{\mathrm{el}}} \sum_{Z=0} N_Z^{\mathrm{gr}} q_Z^{\mathrm{gr-ex}}(T) W_Z^{\mathrm{ex}}$$

$$+ N_Z^{\mathrm{ex}} q_Z^{\mathrm{ex-cont}}(T)(I_Z - W_Z^{\mathrm{ex}}),$$

where $N_Z^{\mathrm{gr}}(t)$ and $N_Z^{\mathrm{ex}}(t)$ are the densities of ions with charge Z in the ground and excited states, respectively; $\tilde{N}_{\mathrm{el}}$ and T are the photoelectron density and temperature after the laser heating; and W_Z^{ex} is the excited-state energy for the ion with charge Z.

Therefore, to determine the ionisation dynamics, we integrate system (4) numerically over the period of a laser pulse, find the photoelectron temperature, and numerically integrate system (5), beginning with the instant of the end of the laser pulse.

The ionisation dynamics calculated upon excitation by a 100-fs Gaussian pulse is presented in Fig. 4a for different peak intensities. Figure 4b shows the experimentally measured radial profile of the refractive index of the femtosecond laser nitrogen microplasma at the instant of time 500 fs following the primary breakdown (for a peak laser-pulse intensity of 1.7×10^{16} W cm^{-2}) and the result of numerical simulation for the same parameters. One can see that the numerical simulation is in good agreement with the experimentally measured values of the electron density. It should be noted that the special features ('steps') in the calculated profile of the electron density have a characteristic size of less than 0.5 μm, which is substantially smaller than the spatial resolution of the experimental technique. In our experiments the resolution was $\sim$1.5 μm, and so these features were not recorded.

Note that the photoionisation by the picosecond pedestal or the postpulse may have another explanation for the growth of electron density after the end of the laser pulse. The rate of this (multiphoton) postionisation would be strongly dependent on the intensity: for instance, under the conditions of Fig. 3 for nitrogen, it would be proportional to the fourth power of the intensity. However, the observed postionisation dynamics at different distances

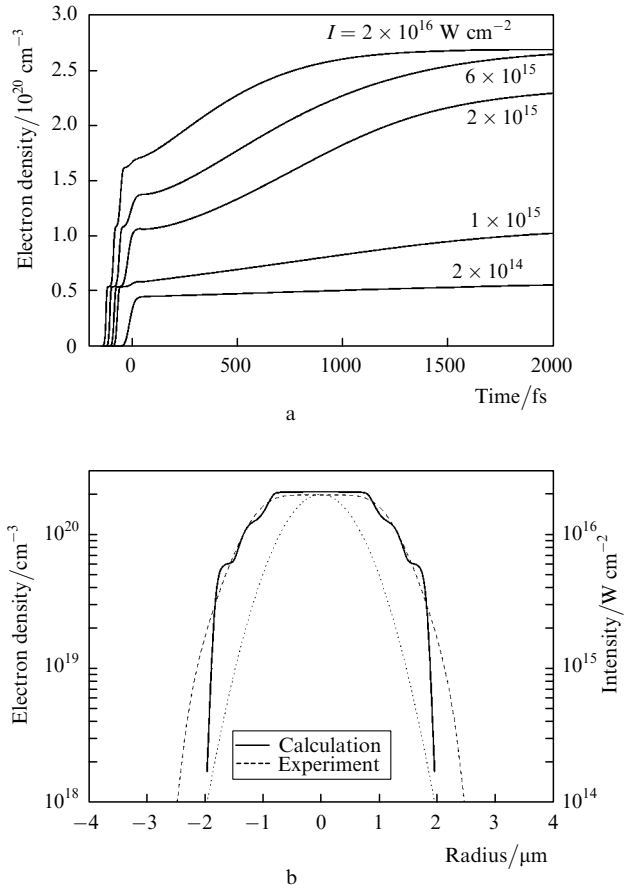

Figure 4. Results of numerical calculation of electron density dynamics of the femtosecond laser plasma proceeding from the proposed theoretical model: the time dependence of the electron density in the waist upon excitation by 100-fs Gaussian pulse for different peak intensities (a) and the radial electron density distribution in the waist measured experimentally 500 fs after the primary breakdown (the dashed lined) and calculated theoretically (the solid line) (b). The dotted line shows the radial distribution of the peak laser intensity.

from the beam axis suggests that the intensity dependence is substantially weaker. Therefore, in our experiments this mechanism is not the controlling one. The interaction between the generated microplasma and the probe pulse also cannot lead to an appreciable change in the electron density due to the extremely low probe radiation intensity (below 10^{10} W cm^{-2}).

4. Conclusions

By using the technique of ultrahigh-speed microinterferometry of a femtosecond laser plasma, we have obtained the spatiotemporal profiles of the refractive index and electron density in the plasma generated in gases (air, nitrogen, argon, and helium) upon optical breakdown produced by high-intensity 400-nm, 100-fs, $I \leqslant 4 \times 10^{16}$ W cm^{-2} second-harmonic pulses from a Ti : sapphire laser. The electron density in this plasma was observed to grow certainly after the action of the exciting laser pulse. The theoretical model has been developed describing the postionisation dynamics; the theoretical calculations are in good agreement with the experimental data.

Acknowledgements. The authors thank S.A. Maiorov for discussions of several theoretical problems. This work was performed within the framework of the 'Femtosecond Optics and New Optical Materials' Program of the Presidium of the Russian Academy of Sciences and the 'Optical Spectroscopy and Frequency Standards' Program of the Physical Sciences Division of the Russian Academy of Sciences and supported by the Russian Foundation for Basic Research (Grant Nos 06-02-17014 and 05-02-17627-a), as well as the Foundation for the Promotion of Domestic Science and the 'Dinastiya' Foundation.

References

1. Bukin V.V., Vorob'ev N.S., Garnov S.V., Konov B.I., Lozovoi V.I., Malyutin A.A., Shchelev M.Ya., Yatskovskii I.S. *Kvantovaya Elektron.*, **36** (7), 638 (2006) [*Quantum Electron.*, **36** (7), 638 (2006)].
2. Garnov S.V., Konov B.I., Malyutin A.A., Tsar'kova O.G., Yatskovskii I.S., Dausinger F. *Kvantovaya Elektron.*, **33** (9), 758 (2003) [*Quantum Electron.*, **33** (9), 758 (2003)].
3. Garnov S.V., Konov V.I., Malyutin A.A., Tsarkova O.G., Yatskovsky I.S., Dausinger F. *Laser Phys.*, **13** (3), 386 (2003).
4. Garnov S.V., Bukin V.V., Vorobiev N.S., Malyutin A.A., Konov V.I., Schelev M.Ya. *Techn. Dig. Int. Conf. on Coherent and Nonlinear Optics (ICONO/LAT'2005)* (St. Petersburg, 2005) IWJ2.
5. Garnov S.V., Bukin V.V., Malyutin A.A., Konov V.I., Vorobiev N.S., Schelev M.Ya. *Proc. Int. Symp. on Topical Problems of Nonlinear Wave Physics (NWP-2005)* (St. Petersburg, N. Novgorod, 2005) p. 45.
6. Garnov S.V., Konov V.I., Lozovoi V.I., Malyutin A.A., Schelev M.Ya., Vorobiev N.S. *Conf. Programm of Int. Symp. on Modern Problems of Laser Physics (MPLP'04)* (Novosibirsk, 2004).
7. Garnov S.V., Konov V.I., Lozovoi V.I., Malyutin A.A., Schelev M.Ya., Vorobiev N.S. *Proc. SPIE Int. Soc. Opt. Eng.*, **5580**, 811 (2005).
8. Belland P., De Michelis C., Mattioli M. *Opt. Commun.*, **3**, 7 (1971).
9. Attwood D.T., Coleman L.W. *Appl. Phys. Lett.*, **24**, 408 (1974).
10. Azechi H., Oda S., Tanaka K., Norimatsu T., Sasaki T., Yamanaka T., Yamanaka C. *Phys. Rev. Lett.*, **39**, 1144 (1977).
11. Attwood D.T., Sweeney D.W., Auerbach J.M., Lee P.H.Y. *Phys. Rev. Lett.*, **40**, 184 (1978).
12. Attwood D.T. *IEEE J. Quantum Electron.*, **14** (12), 909 (1978).
13. Raven A., Willi O. *Phys. Rev. Lett.*, **43**, 278 (1979).
14. Vlasov N.G., Korchazhkin S.V., Matsonashvili R.B., Petryakov V.M., Sobolev S.S., Chalkin S.F. *Opt. Spektrosk.*, **59** (4), 934 (1985).
15. Da Silva L.B., Barbee T.W., Cauble R. Jr, Celliers P., Ciarlo D., Libby S., London R.A., Matthews D., Mrowka S., Moreno J.C., Ress D., Trebes J.E., Wan A.S., Weber F. *Phys. Rev. Lett.*, **74**, 3991 (1995).
16. Shao Y.L., Ditmire T., Tisch J.W.G., Springate E., Marangos J.P., Hutchinson M.H.R. *Phys. Rev. Lett.*, **77**, 3343 (1996).
17. Sarkisov G.S., Bychenkov V.Yu., Novikov V.N., Tikhonchuk V.T., Maksimchuk A., Chen S.-Y., Wagner R., Mourou G., Umstadter D. *Pis'ma Zh. Eksp. Teor. Fiz.*, **66** (12), 787 (1997).
18. Ditmire T., Gumbrell E.T., Smith R.A., Djaoui A., Hutchinson M.H.R. *Phys. Rev. Lett.*, **80** (4), 720 (1998).
19. Breitling D., Schittenhelm H., Berger P., Dausinger F., Hugel H. *Appl. Phys. A*, **69**, S505 (1999).
20. Sarkisov G.S., Bychenkov V.Yu., Novikov V.N., Tikhonchuk V.T., Maksimchuk A., Chen S.-Y., Wagner R., Mourou G., Umstadter D. *Phys. Rev. E*, **59**, 7042 (1999).
21. Edwards M.J., MacKinnon A.J., Zweiback J., Shigemori K., Ryutov D., Rubenchik A.M., Keilty K.A., Liang E., Remington B.A., Ditmire T. *Phys. Rev. Lett.*, **87**, 085004 (2001).
22. Couairon A., Berge L. *Phys. Rev. Lett.*, **88**, 135003-1 (2002).

23. Smith R.F., Dunn J., Nilsen J., Shlyaptsev V.N., Moon S., Filevich J., Rocca J.J., Marconi M.C., Hunter J.R., Barbee T.W. *Phys. Rev. Lett*., **89**, 065004-1 (2002).
24. Garnov S.V., Malyutin A.A., Tsarkova O.G., Konov V.I., Dausinger F. *Proc. SPIE Int. Soc. Opt. Eng*., **4637**, 31 (2002).
25. Kim K.Y., Alexeev I., Milchberg H.M. *Opt. Express*, **10** (26), 1563 (2002).
26. Tang H., Guilbaud O., Jamelot G., Ros D., Klisnick A., Joyeux D., Phalippou D., Kado M., Nishikino M., Kishimoto M., Sukegawa K., Ishino M., Nagashima K., Daido H. *Appl. Phys. B*, **78**, 975 (2004).
27. Richardson M., Koay C.-S., Takenoshita K., Keyser C., Bernath R., George S., Teerawattansook S. *Proc. SPIE Int. Soc. Opt. Eng*., **5580**, 434 (2005).
28. Giulietti A., Galimberti M., Gamucci A., Giulietti D., Gizzi L., Koester P., Laate L., Tomassini P., Vaselli M. *Techn. Dig. Int. Conf. on Coherent and Nonlinear Optics (ICONO/LAT'2005)* (St. Petersburg, 2005) IWJ3.
29. Takeda M., Ina H., Kobayashi S. *J. Opt. Soc. Am*., **72**, 156 (1982).
30. Nugent K. *Appl. Opt*., **24**, 3101 (1985).
31. Born M., Wolf E. *Principles of Optics* (Oxford: Pergamon Press, 1969; Moscow: Nauka, 1973).
32. Landau L.D., Lifshits E.M. *Quantum Mechanics: Non-Relativistic Theory* (Oxford: Pergamon Press, 1977; Moscow: Nauka, 1989).
33. Bauer D., Mulser P. *Phys. Rev. A*, **59**, 569 (1999).
34. Balakin A.A., Fraiman G.M. *Zh. Eksp. Teor. Fiz*., **120**, 797 (2001).
35. Maiorov S.A. *Fiz. Plazmy*, **27** (4), 311 (2001).
36. Brantov A., Rozmus W., Sydora R., Capjack C.E., Bychenko V.Yu., Tikhonchuk V.T. *Phys. Plasmas*, **10**, 3385 (2003).
37. Rascol G., Bachau H., Tikhonchuk V.T., Kull H.-J., Ristow T. *Phys. Plasmas*, **13**, 103108 (2006).
38. Falk R.A., Stefani G., Camilloni R., Dunn G.H., Phaneuf R.A., Gregory D.C., Crandall D.H. *Phys. Rev. A*, **28**, 91 (1983).
39. Moores D.L., Nussbaumer H. *Space Sci. Rev*., **29**, 379 (1981).
40. Crandallf D.H., Phaneuft R.A., Hasselquistl B.E., Gregory D.C. *J. Phys. B: At. Mol. Opt. Phys*., **12**, 7 (1979).
41. Rinn K., Gregory D.C., Wang L.J., Phaneuf R.A., Muller A. *Phys. Rev. A*, **36**, 595 (1987).
42. Takako Kato. *Atomic Data and Nuclear Data Tables*, **57**, 181 (1994).
43. Hudson C.E., Bell K.L. *Phys. Scripta*, **71**, 268 (2005).
44. Frost R.M., Awakowicz P., Summers H.P., Badnell N.R. *J. Appl. Phys*., **84** (6), 2989 (1998).
45. Stafford R.P., Bell K.L., Hibbert A. *J. Phys. B: At. Mol. Opt. Phys*., **25**, 5449 (1992).
46. Ramsbottom C.A., Berrington K.A., Hibbert A., Bell K.L. *Phys. Scripta*, **50**, 246 (1994).
47. Griffin D.C., Badnell N.R., Pindzola M.S. *J. Phys. B*, **33**, 1013 (2000).
48. Datla R.U., Kunze H.-J. *Phys. Rev. A*, **37**, 4614 (1998).